Materials Research Letters
Publication details, including instructions for authors and subscription information:
http://www.tandfonline.com/loi/tmrl20

Mechanics and Mechanically Tunable Band Gap in Single-Layer Hexagonal Boron-Nitride

Jiangtao Wu[a], Baolin Wang[a], Yujie Wei[a], Ronggui Yang[b] & Mildred Dresselhaus[c]
[a] LNM, Institute of Mechanics, Chinese Academy of Sciences, Beijing 100190, People's Republic of China
[b] Department of Mechanical Engineering, University of Colorado, Boulder, CO 80309, USA
[c] Departments of Physics and Department of Electrical Engineering and Computer Sciences, Massachusetts Institute of Technology, Cambridge, MA 02139, USA
Published online: 30 Jul 2013.

To cite this article: Jiangtao Wu, Baolin Wang, Yujie Wei, Ronggui Yang & Mildred Dresselhaus (2013) Mechanics and Mechanically Tunable Band Gap in Single-Layer Hexagonal Boron-Nitride, Materials Research Letters, 1:4, 200-206, DOI: 10.1080/21663831.2013.824516

To link to this article: http://dx.doi.org/10.1080/21663831.2013.824516

MATERIALS RESEARCH LETTERS

Mater. Res. Lett., 2013
Vol. 1, No. 4, 200–206, http://dx.doi.org/10.1080/21663831.2013.824516

Taylor & Francis
Taylor & Francis Group

www.tandfonline.com/toc/tmrl20/current

Mechanics and Mechanically Tunable Band Gap in Single-Layer Hexagonal Boron-Nitride

Jiangtao Wu[a], Baolin Wang[a], Yujie Wei[a]*, Ronggui Yang[b] and Mildred Dresselhaus[c]

[a]*LNM, Institute of Mechanics, Chinese Academy of Sciences, Beijing 100190, People's Republic of China;*
[b]*Department of Mechanical Engineering, University of Colorado, Boulder, CO 80309, USA;*
[c]*Departments of Physics and Department of Electrical Engineering and Computer Sciences, Massachusetts Institute of Technology, Cambridge, MA 02139, USA*

(*Received 3 July 2013; final form 8 July 2013*)

Current interest in two-dimensional materials extends from graphene to others systems such as single-layer hexagonal boron-nitride (h-BN), for the possibility of making heterogeneous structures. Here, we report mechanical properties of h-BN and its band structures tuned by straining by using the density functional theory calculations. Young's modulus and bending rigidity for h-BN are isotropic; its failure strength and failure strain show strong anisotropy. A small fraction of antisite defects in h-BN can largely decrease its mechanical properties. We reveal that strain can tune single-layer h-BN from an insulator to a semiconductor.

Keywords: Hexagonal Boron-Nitride, Anisotropic Strength, Antisite Defects, Mechanical Properties, Band Gap

As another member of the two-dimensional (2D) material family, single-layer hexagonal boron-nitride (h-BN) [1–8] has received increasing attention recently, due to the great similarity between h-BN and graphene and the potential to be heterogeneously integrated with graphene electronics. Graphene and h-BN resemble one another in many aspects, e.g. the capability to form tubes,[2,9] a honey comb arrangement in sp^2-bonded 2D layers, high thermal conductivity and excellent lubrication properties. Furthermore, they also exhibit significant differences: in contrast to its rival graphene with no band gap and being a semi-metal,[10–12] h-BN is electrically insulating with a large band gap both within and across the layers due to the ionic bonding between B and N through charge transfer from B to N.[13] Such striking differences in physical properties stimulate great interest in the heterogeneous integration of both materials for multi-functional applications.[10,14] For example, there is growing interest to tune the band gaps of 2D materials by adopting hybrid structures to utilize the large band gap of h-BN and the zero band gap of graphene to potentially realize a target band gap.[15–17] Now it has been revealed that mechanical strains can tune the band gaps of h-BN nanoribbons (h-BNNR).[18] This justifies the course to re-examine h-BN for all the extraordinary properties observed in graphene. For example, the mechanical properties of h-BN sheets, h-BN tubes and the defects in h-BN sheets have been investigated.[7,19–24] However, a thorough investigation of the mechanical properties of single-layer h-BN and how mechanics may influence the band structures of h-BN are still missing. Peng et al. have investigated the uniaxial tensile and compressive stress–strain response of h-BN [24] with deformation in the transverse being constrained to some extent. The mechanical strength of h-BN in pure uniaxial tension, i.e. when the stress component in the transverse direction is fully relaxed to be zero, remains unknown. Furthermore, it is recognized that the presence of defects in graphene can significantly alter the mechanical and electrical properties of graphene [25–28]; therefore, it is critical to understand how defects affect the properties of h-BN if these defects present in h-BN. In this work, we perform a systematic investigation on several critical mechanical properties of single-layer h-BN, including Young's modulus, the Poisson's ratio, bending rigidity, the mechanical properties of h-BN with antisite defects and the band structure tunability by mechanical strain.

First principles density functional theory (DFT) calculations on single-layer h-BN were performed with the Vienna Ab initio Simulation Package (VASP) code.

*Corresponding author. Email: yujie_wei@lnm.imech.ac.cn

[29,30] The projector-augmented wave pseudopotentials [31,32] and the generalized gradient approximation of the Perdew–Burke–Ernzerhof (PBE) functional [33,34] are used. A plane-wave basis set with a kinetic-energy cut-off of 400 eV and a Monkhorst-Pack (M-P) [35] k-point mesh of $31 \times 31 \times 1$ are used for static electronic structure calculations. One hundred and one uniformly spaced k-points between two high symmetrical points are used in the non-self-consistent calculation to obtain the band structure. An M-P k-point mesh of $1 \times 1 \times 15$ was used for the structure of single-wall h-BN tubes with chiral index $(n = 5, m = 0)$ in the mechanical property calculations. To eliminate the interactions between periodic images of h-BN sheets, a vacuum space of 20 Å was used. Periodic boundary conditions are applied to the two in-plane directions in all the calculations conducted here. All structures are relaxed using a conjugate gradient algorithm until the atomic forces converge to 0.01 eV/Å.

Following the rules to define the chirality of carbon nanotubes and graphene, the orientation of a single-layer crystalline h-BN is described by two unit vectors $\boldsymbol{a}_1$ and $\boldsymbol{a}_2$, and h-BN has a chiral vector $\boldsymbol{C}_h = n\boldsymbol{a}_1 + m\boldsymbol{a}_2$, as illustrated in Figure 1(a). Mechanical loading is applied to four different orientations in h-BN, as defined by chiralities: (i) zigzag $\boldsymbol{C}_h = (1, 0)$; (ii) armchair $\boldsymbol{C}_h = (1, 1)$; (iii) $\boldsymbol{C}_h = (4, 1)$; and (iv) $\boldsymbol{C}_h = (2, 1)$, such that θ, which is the angle between the loading direction (vector $\boldsymbol{C}_h$) and the zigzag direction ($\boldsymbol{a}_1$), changes from 0° to 30° with an increment of about 10°. In the calculations, we first fully relax the unit cell to determine the equilibrium lattice constant, and a lattice constant of $a = 2.504$ Å is found, which agrees well with the experimental measurement of 2.506 Å.[36] Except for the bi-axial loading case, we relax the box in the direction perpendicular to the loading axis in the sheet plane in all other calculations. To obtain the equivalent stress of the single-layer h-BN, an interlayer distance $h_0 = 3.3$ Å [36–41] is used, following reference.[42] We note that current thicknesses for 2D materials are derived based on their three-dimensional counterparts. At this moment, it is an open question whether the thickness of 2D materials with one-atom layer should be redefined. To make the mechanical properties of h-BN easy to be understood, we assume a constant thickness for single-layer h-BN, which results in the usage of engineering stress and engineering strain.

Figure 1(b) shows the engineering stress versus engineering strain curves for the samples subjected to loading in the four directions defined by chiral vectors $\boldsymbol{C}_h$, as mentioned above. In all cases, h-BN exhibits linear elastic response until a strain of about 8%, followed by a nonlinear elastic behaviour until its strength reaches a plateau. Table 1 summarizes Young's modulus, the strength, the failure strain corresponding to the point at the strength, as well as the critical bond length at failure.

Similar to the mechanical properties of graphene,[24, 41] we find that the strength and the failure strain in h-BN are strongly anisotropic. The strength and failure strain when pulling along the zigzag direction is much higher than that along the armchair direction. This can be well explained by the honey comb sp^2-bonded atomic arrangement. The maximum distance of two neighboring planes parallel to the zigzag direction is $d_{ZZ} = a/\sqrt{3} = 1.446$ Å, while the distance between atomic planes parallel to the armchair direction is $d_{AC} = a/2 = 1.252$ Å, where $a = 2.504$ Å is the lattice constant of h-BN. Figure 1(c) shows Poisson's ratio as a function of the tensile strain applied. Compared to the isotropic Young's modulus, Poisson's ratio is anisotropic. The Poisson's ratio is defined as $v = ((L_T - L0_T)/(L_{Ch} - L0_{Ch}))L0_{Ch}/L0_T$, where $L0_T$ and $L0_{Ch}$ are the initial lengths of the unit cell in the directions perpendicular and parallel to the loading axis, respectively, while L_T and L_{Ch} are the corresponding ones after an applied strain. As seen from Figure 1(c), Poisson's ratio under small strain increases with increasing strain. However, when a larger strain of more than 3% is applied, Poisson's ratio decreases almost linearly with the tensile strain. We further notice that the change in Poisson's ratio by straining in the armchair direction is more significant than that by straining in the zigzag direction. With θ increasing from 0° to 30° (the chiral vector changes from zigzag to armchair), Poisson's ratio decreases from a value of 0.23 in the zigzag direction to 0.17 at 20%

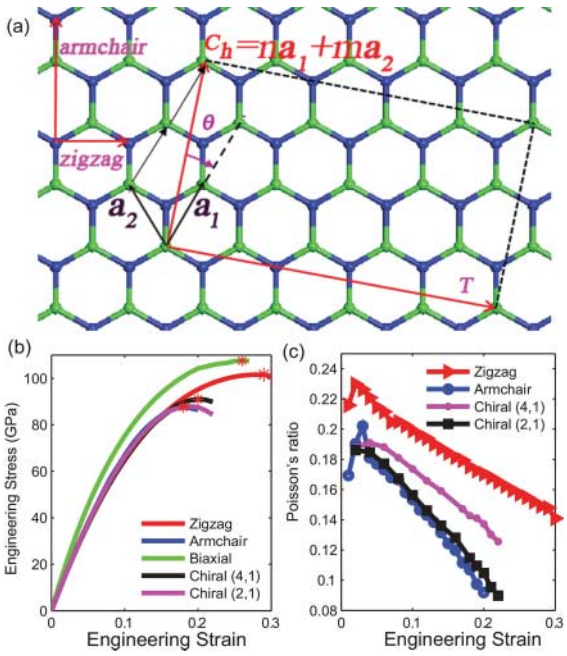

Figure 1. (Color online) Mechanical behavior of h-BN. (a) Definition of orientations in single-layer h-BN. Here, $\boldsymbol{a}_1$ and $\boldsymbol{a}_2$ are the unit vectors of h-BN in real space. A typical rectangular sample (with $\boldsymbol{C}_h = (2, 1)$) for strain–stress calculations was used. (b) Engineering stress vs. engineering strain curves obtained for samples loaded along different directions. (c) Poisson's ratio as a function of engineering strain for different loading cases as described in the text.

Table 1. Mechanical properties of single-layer h-BN when mechanical strain is applied in different directions.

Loading orientation	Chirality	θ	Young's modulus (GPa)	Strength (GPa)	Critical strain	Critical bond length (Å)
Zigzag	(1,0)	0	780 ± 20	102	0.29	1.751
Rotated	(4, 1)	10.9	782 ± 20	91	0.20	1.751
Rotated	(2, 1)	19.1	780 ± 20	88	0.19	1.756
Armchair	(1,1)	30	773 ± 40	88	0.18	1.760
Bi-axial	/	/	995 ± 60	108	0.21	1.821

Note: Here the strength and the critical strain are the maximum stress and the corresponding strain from the stress–strain curves in Figure 1(b), respectively.

strain, while that in the armchair direction changes from 0.20 to about 0.09. Young's modulus and Poisson's ratio v at lower strain reported here are comparable with previous investigations.[19,24]

The antisite defects are uniquely seen in h-BN and have long been investigated by experiments [43,44] and theory.[13,45–48] However, the effects of antisite defects on the mechanical properties of h-BN remain unclear. By applying DFT calculations, we investigated the mechanical behaviour of two types of antisite defects in h-BN. Figure 2(a) and 2(b) shows the unit cell of h-BN containing 96 atoms with a nitrogen antisite and a boron antisite, respectively, used in our calculations. The in-plane dimensions are 15.0008 Å × 17.3216 Å for the structure with a boron antisite and 15.0756 Å × 17.4075 Å for the sample with a nitrogen antisite. Such a large sample can effectively minimize the interaction of defects in the periodical image. We also mark the bond lengths near the defects in Figure 2(a) and Figure 2(b) after structure relaxation. The B−B bond in the h-BN structure in Figure 2(a) is much longer than the B−N bond and on the contrary, the N−N bond in the h-BN structure in Figure 2(b) is much shorter than its neighboring B−N bond. These changes may account for the decrease in the tensile strength of h-BN, as seen from Figure 2(c). By comparing the results of Figure 2(c) with that in Figure 1(b), we see that the strengths of an intact h-BN in the armchair and zigzag are 88 and 102 GPa, respectively, corresponding strengths in h-BN with a boron antisite are 86 and 93 GPa, and those in h-BN with a nitrogen antisite are 80 and 92 GPa. While there is only one-ninety-sixth change in atomic composition, the strength change can be as high as 10%. The presence of these antisite defects will largely decrease the mechanical performance. Figure 2(d) shows Poisson's ratio versus engineering strain curves, respectively, for h-BN with antisite defects, which are similar to those in intact samples. Poisson's ratio decreases linearly with increasing engineering strain.

Two-dimensional h-BN and graphene not only have high modulus and tensile strength but also have extremely small out-of-plane stiffness given the material is the ultimate thin membrane. Such a combination of mechanical properties makes them ideal candidates for

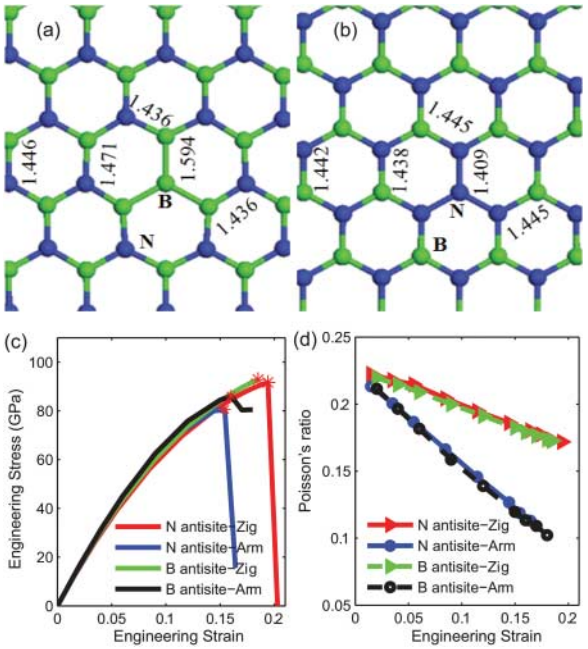

Figure 2. (Color online) H-BN structures with antisite defects and their mechanical behaviors. (a) h-BN structure with a nitride antisite defect. (b) h-BN structure with a boron antisite defect. (c) Engineering stress vs. engineering strain curves obtained for samples loaded along different directions. (c) Poisson's ratio as a function of engineering strain for different loading cases as described in the text.

biological membranes and stretchable electronics applications. Here, we also studied the bending rigidity B_M of single-layer h-BN, which governs the morphology of 2D materials under external field stimuli. To obtain B_M of single-layered h-BN, we perform DFT calculations to get the energies of single-wall h-BN nanotubes (SWBNT) of different radii. By using the Helfrich Hamiltonian,[48] the bending rigidity of a free-standing single-layer h-BN is then connected with the energy of a B-N pair E_{BN} in SWBNT with the radii r [48,49]:

$$E_{BN} = E_0 + \frac{S_0 B_M r^{-2}}{2}, \quad (1)$$

where E_0 is the energy of one B-N pair in a flat h-BN sheet, and $S_0 = \frac{3\sqrt{3}d^2}{2} = 5.432$ Å^2 is the planar footprint

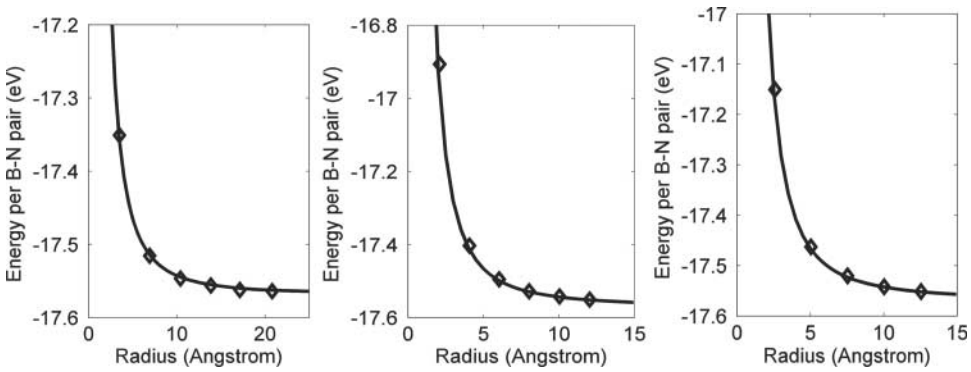

Figure 3. Energy per B-N pair versus the radius in single-wall h-BN tubes with different rolling up directions: DFT calculations (symbols) and the fitted curve obtained by using Equation (1) with bending rigidity $B_M = 0.95$ eV (solid lines). (a) For tubes rolled up along the armchair direction. (b) For tubes rolled up along the zigzag direction. (c) For tubes rolled up along the (5, 2) chirality.

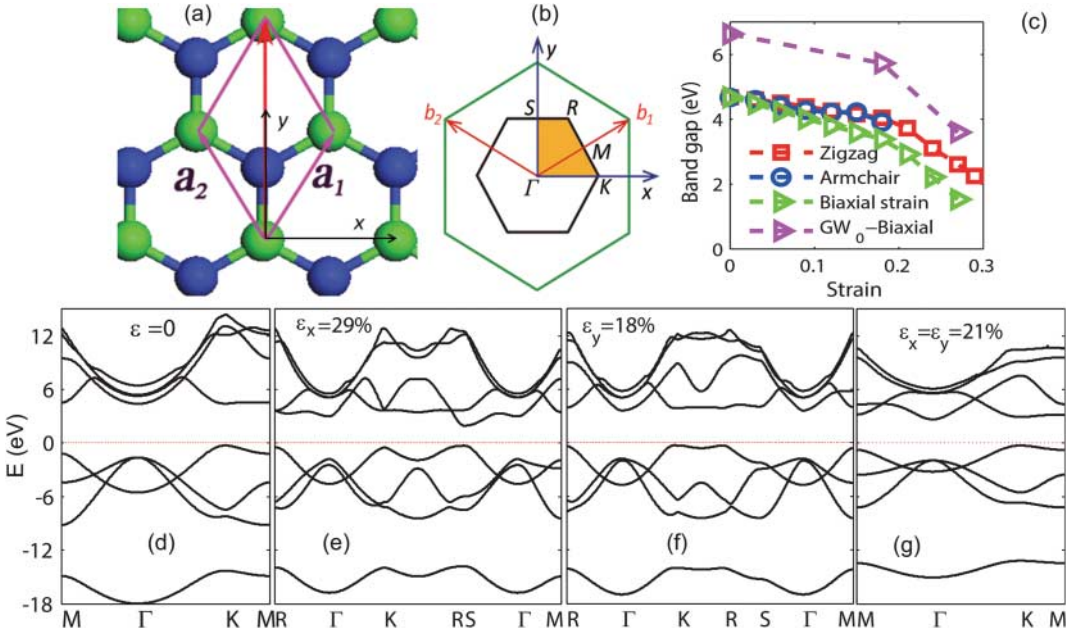

Figure 4. (Color online): Band structures and band gap of h-BN in response to engineering strains. (a) The two-atom unit cell used for band structure calculations (in the red box). (b) Corresponding reciprocal lattice and the first Brillouin zone. (c) Band gaps as a function of engineering strains for different loading directions calculated by suing DFT-PBE and ScGW$_0$ method. (d) The DFT band structure of monolayer h-BN in the absence of strain. (e)–(g), the DFT band structures at corresponding critical strains along different directions: (e) at 29% strain along the zigzag direction, (f) at 18% strain along the armchair direction and (g) at 21% bi-axial strain.

of a B-N pair where the B-N bond length is $d = 1.446$ Å. In the absence of deformation, E_0 for single-layer h-BN is calculated to be -17.568 eV using DFT. The dots in Figure 3 are the energies per B-N pair for different radii in SWBNT based on DFT calculations, with Figure 3(a)–(c) corresponding to zigzag tubes, armchair tubes and tubes rolled up along the $\boldsymbol{C}_h = (5, 2)$ direction. The solid line in Figure 3 shows the prediction of Equation (1), by using a bending rigidity of 0.95 eV. A single value of bending rigidity 0.95 eV in Equation (1) can describe very well the dependence of E_{BN} on tube radii r, regardless of the roll-up direction of the h-BN tubes, indicating the isotropic nature of the bending rigidity for single-layer h-BN. We note that the bending rigidity of h-BN tubes was also reported in reference,[18] where the author showed slight difference in the bending rigidity of h-BN in different directions. What we report here for isotropic bending property in h-BN is consistent with the prediction by elasticity theory that trigonal symmetry crystals in 2D have isotropic bending properties.[50]

In addition to the extraordinary mechanical properties like graphene, the electrical properties of h-BN make it special: graphene is gapless and h-BN is an insulator. This distinct property stimulates great interest in finding

effective ways to tune the electrical and magnetic properties of such 2-D materials.[51–53] For example, it is known that mechanical straining can alter the band gaps of graphene nanoribbons significantly.[51,54–59] Similarly, it has also been shown that straining can change the band gaps for h-BN nanoribbons [15,18] and large area h-BN.[60] We note that in reference,[60] the authors investigated the bandgap as a function of strain to the strain where the bandgap eventually approaches zero. Here, we repeat these calculations to a realistic strain level where further straining would break the sample, and determine the real smallest bandgap we can achieve by applying strains to h-BN. We explore the dependence of the band gap on mechanical straining in large h-BN samples. Figure 4(a) shows the two-atom unit cell used for band structure calculations with Figure 4(b) showing the corresponding reciprocal lattice and the first Brillouin zone. Figure 4(d) shows the band structure of single-layer h-BN in the absence of strain. An indirect band gap of 4.7 eV is obtained, which is in good agreement with the former DFT calculation result obtained using the local density approximation,[61,62] but lower than that from calculations obtained by using the quasiparticle Green's function and the screened Coulomb interaction approximation (GWA) (5.95 eV).[63] Figure 4(e)–4(g), in turn, shows the band structures of single-layer h-BN when the critical uni-axial strain is applied along the zigzag direction, along the armchair direction, and bi-axially. Very different from graphene, which has been shown that mechanical strain has very little effect on the band structure of large-area graphene,[64,65] the band gap of h-BN decreases dramatically with increasing tensile strain. A summary of the band gap as a function of different values of the strain in the three typical directions is given in Figure 4(c). There exist two regions where we see a linear dependence of band gap on strains: the band gap decreases slowly with the increasing strain when the applied strain is smaller than 18%; but showing a quicker decrease when a strain larger than 18% is applied. Such a dependence of band gap on straining is also seen to be anisotropic: the band gap is more sensitive to the applied bi-axial strains than to the two applied uni-axial strains. To verify whether the band gap can be largely reduced by strain, we further use more accurate GWA to get the band gap of h-BN subjected to bi-axial strain. The $scGW_0$ calculations are performed by using VASP. A Monkhorst-Pack k-point mesh of $12 \times 12 \times 1$ in BZ and 128 bands are used. The energy cut-off for the response function is chosen to be 200 eV. The results show that the single-layer h-BN is an indirect band gap material with a band gap energy of 6.63 eV, which is larger than the result from all-electron GWA (5.95 eV) [63] and some experiments (5.5–5.97 eV) [7,10,66]. When bi-axial strains of 18% and 27% are applied, the band gap of h-BN reduces to 5.73 eV (direct band gap) and 3.6 eV (indirect band gap), as shown in Figure 4(c).

In summary, we investigated several critical mechanical properties of single-layered h-BN by using DFT calculations. We find that Young's modulus of single-layered h-BN is about 780 GPa and is nearly independent of crystalline orientation. The bending rigidity is also isotropic and is about 0.95 eV. Nevertheless, the failure behaviour and Poisson's ratio of h-BN are highly anisotropic. A small fraction of antisite defects in h-BN can largely decrease its mechanical strength and failure strain. In addition, we investigated the band structures of single-layered h-BN as a function of different mechanical straining, and we found that there is a bi-linear dependence of band gap on the applied tensile strains. Mechanical strain can tune the band gap of single-layer h-BN from an insulator to a semiconductor, which implies the potential electronic application of single-layer h-BN.

Acknowledgements Y. W. acknowledges the support from Chinese Academy of Sciences (CAS), MOST 973 of China (Nr. 2012CB937500), and National Natural Science Foundation of China (NSFC) (11021262, 11272327). R. Y. acknowledges the support from AFOSR (Grant No. FA9550-11-1-0109). M. D. acknowledges the support of the Solid State Solar-Thermal Energy Conversion Center (S3TEC), an Energy Frontier Research Center funded by the U.S. Department of Energy, Office of Science, Office of Basic Energy Sciences under Award Number: DE-SC0001299/DE-FG02-09ER46577. All calculations are performed at the Supercomputing Center of CAS.

References

[1] Novoselov KS, Jiang D, Schedin F, Booth TJ, Khotkevich VV, Morozov SV, Geim AK. Two-dimensional atomic crystals. Proc Natl Acad Sci USA. 2005;102(30):10451–10453.

[2] Chopra NG, Luyken RJ, Cherrey K, Crespi VH, Cohen ML, Louie SG, Zettl A. Boron nitride nanotubes. Science. 1995;269(5226):966–967.

[3] Pacilé D, Meyer JC, Girit CO, Zettl A. The two-dimensional phase of boron nitride: few-atomic-layer sheets and suspended membranes. Appl Phys Lett. 2008;92(13):133107.

[4] Meyer JC, Chuvilin A, Algara-Siller G, Biskupek J, Kaiser U. Selective sputtering and atomic resolution imaging of atomically thin boron nitride membranes. Nano Lett. 2009;9(7):2683–2689.

[5] Jin C, Lin F, Suenaga K, Iijima S. Fabrication of a freestanding boron nitride single layer and its defect assignments. Phys Rev Lett. 2009;102(19):195505.

[6] Alem N, Erni R, Kisielowski C, Rossell M, Gannett W, Zettl A. Atomically thin hexagonal boron nitride probed by ultrahigh-resolution transmission electron microscopy. Phys Rev B. 2009;80(15):155425.

[7] Song L, Ci L, Lu H, Sorokin PB, Jin C, Ni J, Kvashnin AG, Kvashnin DG, Lou J, Yakobson BI, Ajayan PM. Large scale growth and characterization of atomic hexagonal boron nitride layers. Nano Lett. 2010;10(8):3209–3215.

[8] Sutter P, Cortes R, Lahiri J, Sutter E. Interface formation in monolayer graphene-boron nitride heterostructures. Nano Lett. 2012;12(9):4869–4874.

[9] Iijima S. Helical microtubules of graphitic carbon. Nature. 1991;354(6348):56–58.

[10] Watanabe K, Taniguchi T, Kanda H. Direct-bandgap properties and evidence for ultraviolet lasing of hexagonal boron nitride single crystal. Nat Mater. 2004;3(6):404–409.

[11] Novoselov KS, Geim AK, Morozov SV, Jiang D, Zhang Y, Dubonos SV, Grigorieva IV, Firsov AA. Electric field effect in atomically thin carbon films. Science. 2004;306(5696):666–669.

[12] Novoselov KS, Geim AK, Morozov SV, Jiang D, Katsnelson MI, Grigorieva IV, Dubonos SV, Firsov AA. Two-dimensional gas of massless Dirac fermions in graphene. Nature. 2005;438(7065):197–200.

[13] Topsakal M, Aktürk E, Ciraci S. First-principles study of two- and one-dimensional honeycomb structures of boron nitride. Phys Rev B. 2009;79(11):115442.

[14] Kubota Y, Watanabe K, Tsuda O, Taniguchi T. Deep Ultraviolet light-emitting hexagonal boron nitride synthesized at atmospheric pressure. Science. 2007;317(5840):932–934.

[15] Ramasubramaniam A, Naveh D, Towe E. Tunable band gaps in bilayer graphene-BN heterostructures. Nano Lett. 2011;11(3):1070–1075.

[16] Quhe R, Zheng J, Luo G, Liu Q, Qin R, Zhou J, Yu D, Nagase S, Mei W-N, Gao Z, Lu J. Tunable and sizable band gap of single-layer graphene sandwiched between hexagonal boron nitride. NPG Asia Mater. 2012;4(2):e6.

[17] Fan Y, Zhao M, Wang Z, Zhang X, Zhang H. Tunable electronic structures of graphene/boron nitride heterobilayers. Appl Phys Lett. 2011;98(8):083103.

[18] Qi J, Qian X, Qi L, Feng J, Shi D, Li J. Strain-engineering of band gaps in piezoelectric boron nitride nanoribbons. Nano Lett. 2012;12(3):1224–1228.

[19] Kudin K, Scuseria G, Yakobson B. C2F, BN, and C nanoshell elasticity from ab initio computations. Phys Rev B. 2001;64(23):235406.

[20] Golberg D, Bando Y, Huang Y, Terao T, Mitome M, Tang C, Zhi C. Boron nitride nanotubes and nanosheets. ACS Nano. 2010;4(6):2979–2993.

[21] Chopra NG, Zettl A. Measurement of the elastic modulus of a multi-wall boron nitride nanotube. Solid State Commun. 1998;105(5):297–300.

[22] Bettinger H, Dumitricã T, Scuseria G, Yakobson B. Mechanically induced defects and strength of BN nanotubes. Phys Rev B. 2002;65(4):041406.

[23] Liu Y, Zou X, Yakobson BI. Dislocations and grain boundaries in two-dimensional boron nitride. ACS Nano. 2012;6(8):7053–7058.

[24] Peng Q, Ji W, De S. Mechanical properties of the hexagonal boron nitride monolayer: ab initio study. Comput Mater Sci. 2012;56:11–17.

[25] Wei Y, Wu J, Yin H, Shi X, Yang R, Dresselhaus M. The nature of strength enhancement and weakening by pentagon–heptagon defects in graphene. Nat Mater. 2012;11:759–763.

[26] Yazyev OV, Louie SG. Electronic transport in polycrystalline graphene. Nat Mater. 2010;9(10):806–809.

[27] Wu JT, Shi XH, Wei YJ. Tunable band structures of polycrystalline graphene by external and mismatch strains. Acta Mech Sinica. 2012;28(6):1539–1544.

[28] Wu J, Wei Y. Grain. Misorientation and grain-boundary rotation dependent mechanical properties in polycrystalline graphene. J Mech Phys Solids. 2013;61(6):1421–1432.

[29] Kresse G, Furthmüller J. Efficiency of ab-initio total energy calculations for metals and semiconductors using a plane-wave basis set. Comput Mater Sci. 1996;6(1):15–50.

[30] Kresse G, Furthmüller J. Efficient iterative schemes for ab initio total-energy calculations using a plane-wave basis. Set Phys Rev B. 1996;54(16):11169–11186.

[31] Blöchl PE. Projector augmented-wave method. Phys Rev B. 1994;50(24):17953–17979.

[32] Kresse G, Joubert D. From ultrasoft pseudopotentials to the projector augmented-wave method. Phys Rev B. 1999;59(3):1758–1775.

[33] Perdew JP, Burke K, Ernzerhof M. Generalized gradient approximation made simple. Phys Rev Lett. 1996;77(18):3865–3868.

[34] Perdew JP, Burke K, Ernzerhof M. Generalized gradient approximation made simple [Phys Rev Lett. 77, 3865 (1996)]. Phys Rev Lett. 1997;78(7):1396–1396.

[35] Monkhorst HJ, Pack JD. Special points for brillouin-zone integrations. Phys Rev B. 1976;13(12):5188–5192.

[36] Paszkowicz W, Pelka JB, Knapp M, Szyszko T, Podsiadlo S. Lattice parameters and anisotropic thermal expansion of hexagonal boron nitride in the 10–297.5 K temperature range. Appl Phys A. 2002;75(3):431–435.

[37] Shi Y, Hamsen C, Jia X, Kim KK, Reina A, Hofmann M, Hsu AL, Zhang K, Li H, Juang ZY, Dresselhaus MS, Li LJ, Kong J. Synthesis of few-layer hexagonal boron nitride thin film by chemical vapor deposition. Nano Lett. 2010;10(10):4134–4139.

[38] Lin Y, Williams TV, Connell JW. Soluble, exfoliated hexagonal boron nitride nanosheets. J Phys Chem Lett. 2009;1(1):277–283.

[39] Solozhenko VL, Will G, Elf F. Isothermal compression of hexagonal graphite-like boron nitride up to 12 GPa. Solid State Commun. 1995;96(1):1–3.

[40] Hod O. Graphite and hexagonal boron-nitride have the same interlayer distance. Why? J Chem Theory Comput. 2012;8(4):1360–1369.

[41] Marini A, García-González P, Rubio A. First-principles description of correlation effects in layered materials. Phys Rev Lett. 2006;96(13):136404.

[42] Liu F, Ming P, Li J. Ab initio calculation of ideal strength and phonon instability of graphene under tension. Phys Rev B. 2007;76(6):064120.

[43] Peter R, Bozanic A, Petravic M, Chen Y, Fan LJ, Yang YW. Formation of defects in boron nitride by low energy ion bombardment. J Appl Phys. 2009;106(8):083523.

[44] Bozanic A, Petravic M, Fan LJ, Yang YW, Chen Y. Direct observation of defect levels in hexagonal BN by soft X-ray absorption spectroscopy. Chem Phys Lett. 2009;472(4–6):190–193.

[45] Orellana W, Chacham H. Stability of native defects in hexagonal and cubic boron nitride. Phys Rev B. 2001;63(12):125205.

[46] Azevedo S, Kaschny JR, De Castilho CMC, Mota FDB. A theoretical investigation of defects in a boron nitride monolayer. Nanotechnology. 2007;18:495707.

[47] Jimenez I, Jankowski AF, Terminello LJ, Sutherland DGJ, Carlisle JA, Doll GL, Tong WM, Shuh DK, Himpsel FJ. Core-level photoabsorption study of defects and metastable bonding configurations in boron nitride. Phys Rev B. 1997;55(18):12025–12037.

[48] Helfrich W. Elastic properties of lipid bilayers: theory and possible experiments. Z Naturforsch. 1973;28c(11):693–703.

[49] Wei Y, Wang B, Wu J, Yang R, Dunn ML. Bending rigidity and gaussian bending stiffness of single-layered graphene. Nano Lett. 2013;13(1):26–30.
[50] Landau LD, Lifshitz EM. Theory of elasticity. 3rd ed. Oxford: Butterworth-Heinemann; 1986.
[51] Han M, Zyilmaz B, Zhang Y, Kim P. Energy band-gap engineering of graphene nanoribbons. Phys Rev Lett. 2007;98(20):206805.
[52] Beheshtian J, Sadeghi A, Neek-Amal M, Michel K, Peeters F. Induced polarization and electronic properties of carbon-doped boron nitride nanoribbons. Phys Rev B. 2012;86(19):195433.
[53] Machado-Charry E, Boulanger P, Genovese L, Mousseau N, Pochet P. Tunable magnetic states in hexagonal boron nitride sheets. Appl Phys Lett. 2012;101(13): 132405.
[54] Son YW, Cohen ML, Louie SG. Energy gaps in graphene nanoribbons. Phys Rev Lett. 2006;97(21):216803.
[55] Nakada K, Fujita M, Dresselhaus G, Dresselhaus MS. Edge state in graphene ribbons: nanometer size effect and edge shape dependence. Phys Rev B. 1996;54(24):17954–17961.
[56] Brey L, Fertig H. Electronic states of graphene nanoribbons studied with the Dirac equation. Phys Rev B. 2006;73(23):235411.
[57] Chen ZH, Lin YM, Rooks MJ, Avouris P. Graphene nanoribbon electronics. Physica E. 2007;40(2):228–232.
[58] Guinea F, Katsnelson MI, Geim AK. Energy gaps and a zero-field quantum hall effect in graphene by strain engineering. Nat Phys. 2010;6(1):30–33.
[59] Pereira V, Castro Neto A, Peres N. Tight-binding approach to uniaxial strain in graphene. Phys Rev B. 2009;80(4):045401.
[60] Li J, Gui G, Zhong J. Tunable bandgap structures of two-dimensional boron nitride. J Appl Phys. 2008;104(9):094311.
[61] Doni E, Parravicini G. Energy bands and optical properties of hexagonal boron nitride and graphite. IL Nuovo Cimento B. 1969;64(1): 117–144.
[62] Bhattacharya A, Bhattacharya S, Das GP. Band gap engineering by functionalization of BN sheet. Phys Rev B. 2012;85(3):035415.
[63] Arnaud B, Lebègue S, Rabiller P, Alouani M. Huge Excitonic effects in layered hexagonal boron nitride. Phys Rev Lett. 2006;96(2):026402.
[64] Gui G, Li J, Zhong J. Band structure engineering of graphene by strain: first-principles calculations. Phys Rev B. 2008;78(7):075435.
[65] Farjam M, Rafii-Tabar H. Comment on "band structure engineering of graphene by strain: first-principles calculations". Phys Rev B. 2009;80(16): 167401.
[66] Tarrio C, Schnatterly SE. Interband transitions, plasmons, and dispersion in hexagonal boron nitride. Phys Rev B. 1989;40(11):7852–7859.